Isotope-Induced Structural Effects

Compositional and Isotopologue-Induced Phase Differentiation in Supramolecular Aggregates**

*Jaeho Lee and Sergiu M. Gorun**

To date there have been few experimental studies that have probed deuterium effects upon aggregations. In biology, a 1975 report links deuterium effects with the K^+-, Cs^+-, and NH_4^+-induced assembly of tetrameric *Clostridium cylindrosporum* formyltetrahydrofolate synthetase (FTHFS) from monomeric units.[1] Monomer association is enhanced 50-fold in D_2O due, at least in part, to the 2.8-fold increase in the FTHFS monomer–alkaline cation association constant in D_2O. The hydrated cations are coordinated by the carboxylato and carbonyl oxygen atoms of amino acids, as revealed recently.[2] The assembly of inorganic aggregates that exhibit controlled topologies and nuclearities, remains a challenge for the synthetic chemist.

We have recently reported the discovery of a novel structural (thermodynamic) hydrogen isotope effect, and provided examples of isotope-dependent formation of Mn and Fe aggregates in inorganic and bioinorganic chemistry.[3] In the Mn case, repeated preparations in H_2O and D_2O have revealed the formation of similar Mn_{16} units, aggregated further in supramolecular assemblies by additional Cl^- and hydrated Na^+ and Ba^{2+} ions. Four peripheral Ba^{2+} ions, present in the Mn_{16} aggregates obtained from both H_2O and D_2O, are coordinated by water and carbonyl oxygen atoms. In the D_2O case, but not in the H_2O case, Cl^- ions are hydrogen-bonded to deuteroxo groups that bridge two Mn centers, while water molecules of hydration coordinate additional Ba^{2+} ions, which, in turn, are linked to Na^+ ions by extra water molecules (Figure 1).

Despite identical Na/Cl/Ba solution concentrations, the Mn_{16} phases obtained from D_2O, P3 (L = the pentaanion of 1,3-diamino-2-hydroxypropane-*N,N,N′,N′*-tetraacetic acid), contain two extra Na^+, Cl^-, and Ba^{2+} ions relative to the Mn_{16} phases obtained from H_2O, P1.[3] The extra four charges in P3 require four fewer deuterons and/or lower average Mn oxidation states (maximum four units) for overall charge neutrality. The high, 4/*m* symmetry of the aggregates, however, precludes a precise determination of these differences by X-ray diffraction.[4]

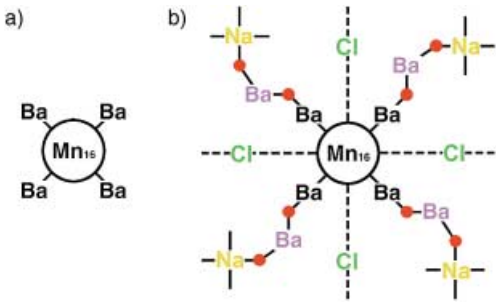

Figure 1. Schematic representation of a) the peripheral Ba^{2+} ions linked directly to the Mn_{16} aggregate from H_2O, phase P1, and b) the additional Ba^{2+} and Na^+ ions linked to the first set through bridging D_2O molecules (shown as dots), phase P3.

$$[Mn_{16}O_4(OD)_4(CO_3)_4L_8Ba_{10\pm0.5}Na_{4\pm1}Cl_3]\cdot 80\pm3\,D_2O \quad P3$$

$$[Mn_{16}O_4(OH)_4(CO_3)_4L_8Ba_8Na_2Cl]\cdot 54\pm8\,H_2O \quad P1$$

The reasons for isotopologue-dependent formation of different aggregates, starting with solutions of otherwise identical compositions, are not fully understood.

We report here the discovery of correlations between the variable *concentration* of NaCl in H_2O and D_2O solutions and the type *and number* of solid-state phases derived from them, correlations that are dependent on the hydrogen isotopologue. Surprisingly, a new, structurally intermediate phase is observed in H_2O, but not in D_2O, a phenomenon reminiscent of the formation of the ice IV structure for D_2O, but not for H_2O.[5]

All Mn_{16} phases were prepared following the procedure in reference [3]. Considering the higher NaCl content of the D_2O phase P3, we wondered if this aggregate could also be produced in H_2O by increasing the NaCl concentration. To this end, the concentration of NaCl in H_2O was varied from about 0.5 to about 5.0 g per 20 mL solution, while maintaining the concentrations of all other reagents, as well as the reaction conditions, constant (see Experimental Section). This procedure amounts to a NaCl "titration". The solids were characterized by X-ray diffraction studies (several single crystals per batch), and the unit cells of the bulk materials were verified by powder X-ray diffraction.

The results, summarized schematically in Figure 2, incorporate the single-point concentration of 1.0 g NaCl per 20 mL solution.[3] As seen in Figure 2 (upper trace), phase P3 is indeed obtained in H_2O, but only when the NaCl concen-

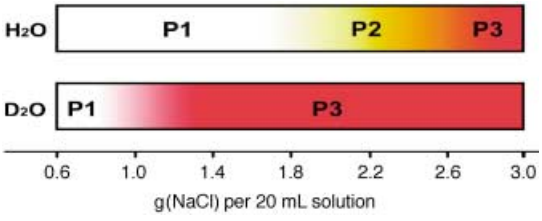

Figure 2. Chart of solid-state Mn_{16} phases versus the concentration of NaCl in solution. The phase boundaries, as expected, are not clearly defined. Crystalline materials do not form outside the chart NaCl limits.

[*] Prof. Dr. S. M. Gorun, J. Lee
Department of Chemistry
Brown University
Providence, RI 02912 (USA)
Fax: (+1) 401-863-9046
E-mail: sergiu_gorun@brown.edu

[**] The partial financial assistance of the National Science Foundation (DMR-0233811), use of MIT SQUID facility, and contributions of Dr. N. R. Brooks and Dr. V. G. Young, Jr. to the X-ray work, are acknowledged.

Supporting information for this article is available on the WWW under http://www.angewandte.org or from the author.

  DOI: 10.1002/ange.200250200

tration approaches 2.6 g per 20 mL solution.[6a] However, the crystallization becomes more difficult as the concentration of NaCl increases. Phase P3 forms after weeks, as opposed to days in D_2O. In H_2O, phase P1 also crystallizes faster (days).

The simulation of the "D_2O effect" by an enhanced NaCl concentration, prompted us to seek, following the same logic, the reverse "H_2O effect", that is, the formation of the H_2O phase P1 in D_2O. The lower trace of Figure 2 shows that this phase forms in D_2O when the NaCl concentration is *lowered*, approximately below 0.9 g per 20 mL solution.[6b] The phases P1 from H_2O and D_2O are quasi-isomorphous. The phases P3 behave similarly. There are, however, small differences.[7]

Interestingly, these phases contain different amounts of Ba^{2+}, despite the fact that the Ba^{2+} concentration in solution was kept constant. This observation suggests that the variation in the concentration of NaCl suffices for phase selectivity *at constant isotope composition*.

Taken together, the above data indicate that the variation in NaCl concentration simulates the effect of the other, seemingly independent parameter, namely the variation of the hydrogen isotopologue in the aqueous solvent. This parallel, however, is not complete. A new phase, P2, is obtained in H_2O at NaCl concentrations between those required for P1 and P3. The structure comprises two crystallographically distinct Mn_{16} aggregates, both of which exhibit 4/*m* symmetry.[7] The first one, labeled Unit 1, is actually P1. The second one, Unit 2, is also P1, but with an additional 8 Na^+ ions, consistent with the increased NaCl concentration in the solution from which P2 is obtained. However, Cl^- ions, found in P3, are not present in Unit 2. The P2 formula is $\{[Mn_{16}O_4(OH)_4(CO_3)_4L_8Ba_8Na_2Cl]\}\{[Mn_{16}O_4(OH)_4(CO_3)_4L_8Ba_8Na_{10}Cl]\}$, written as {Unit 1}{Unit 2} (Figure 3; see also Figure S2 and S3 in the Supporting Information):

The two unique Mn centers have different average oxidation states and coordination geometries. One Mn center is roughly pentagonally bipyramidal coordinated, with a chelating carbonate ion (one Mn–O bond is drawn in Figure 3 with dashed lines) in the equatorial plane. Bond lengths of about 2.13–2.30 Å, and equatorial angles of about 71–76°, are common for both Unit 2 and Unit 1. Both the coordination type and metal–ligand distances indicate a predominance of Mn^{II} at this site. The μ-alkoxo oxygen atom (Figure 3a) is in the apical position of the coordination polyhedra of both Mn centers, but the second Mn atom is only six-coordinate. For this site, the average equatorial bond length of both Unit 1 and Unit 2 (2.080(3) Å) is shorter than those for the Mn^{II} site, and an axial compression is noted: 1.951(3) and 1.956(3) Å for Unit 1 and Unit 2, respectively. The above parameters characterize a site with a predominant, Jahn–Teller compressed, high-spin Mn^{III} occupancy, while excluding higher oxidation levels. A similar, rare Jahn–Teller distortion, was noted for the same ligand in Mn_4 complexes,[8] as well as P1 and P3 phases.[3] Similar to the case of the latter complexes, the high, 4/*m* symmetry of both Unit 1 and Unit 2, precludes the precise determination of the Mn^{II}/Mn^{III} ratios. Iodometric titrations, however, indicate similar ratios of the oxidation states: 8.0(2)/8.0(2) and 7.8(2)/8.2(2) for P2 and P3, respectively, consistent with the presence in Unit 2 of eight additional Na^+ ions. Thus, there are four average charges per Mn_{16} unit of P2. In P3, these extra charges (relative to P1) are due to two Ba^{2+} ions.

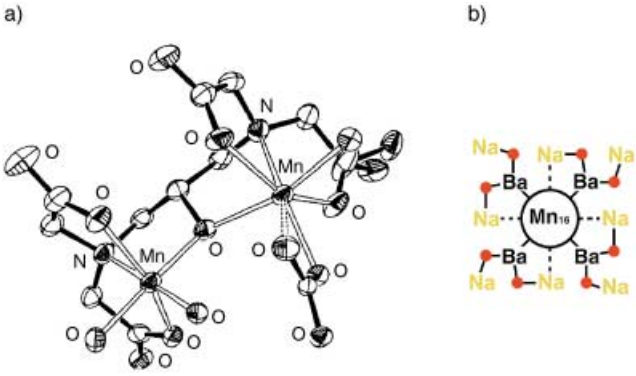

Figure 3. Structures of the Mn_{16} aggregate of Unit 2 of P2. a) The alkoxo-bridged dinuclear Mn center, common to both Unit 2 and Unit 1 and P1 phases (thermal ellipsoids are at 40% probability level; hydrogen atoms and carbon atom labels are omitted for clarity). b) Schematic view down the fourfold axis of the assembly of Unit 2 from phase P1 (Figure 1a) and Na^+ ions. Each dot represents H_2O bridges; the dashed lines represent ligand coordination.

The solid-state packing diagrams of P1, P2, and P3 phases exhibit significant differences (Figure 4). The supramolecular architectures of Mn_{16} building blocks of the three phases are related. Phase P1, which consists only of "pure" building blocks, provides the basic scaffold. In phase P2, every other P1 layer of blocks (see the *ac* plane view) acquires Na^+ ions, but the topology of the blocks remains the same. In phase P3, more interstitial ions are incorporated, resulting in a twist of the building blocks around axes parallel to the *c* direction, and a simultaneous increase and decrease of their spatial density in the *ab* plane and *c* directions, respectively (Figure 4d). As more ions are incorporated, the unit cell volumes *decrease*: P2 and P3 have volumes 95 and 89% of that of P1, respectively. The similarities and differences between the structures of P1 and P2 or P3 are reflected in their magnetic signatures. Variable-temperature magnetic susceptibility measurements of P2 and P3 reveal an overall antiferromagnetic coupling of the Mn ions, characterized by an initial increase of the molar susceptibility (normalized per Mn_{16} unit) as the temperature decreases, and the appearance of soft Néel-type maxima at 10.0 K and 15.6 K for P2 and P3, respectively (see Supporting Information). In both cases, the total spin state values tend toward $S_T = 0$ below 6 K. In contrast, a Néel-type maximum is not observed above 4 K for P1.[3] This data suggests that P2, like P3, is qualitatively different from P1, with manifestations of extended solidlike magnetic behavior, consistent with either different *intra* Mn_{16} aggregate *J* values, or *inter* Mn_{16} aggregate couplings mediated by the peripheral main-group elements. The latter possibility is supported by the above-mentioned enhanced compactness of P2 and P3 relative to P1.

Considering that P1 can also be obtained from D_2O by lowering the NaCl concentration characteristic for P3, it was expected that a P2 phase, like in the case of H_2O, could be obtained from D_2O at intermediate NaCl concentrations. However, we have failed to observe any intermediate phases despite numerous attempts, which suggests that, at least when

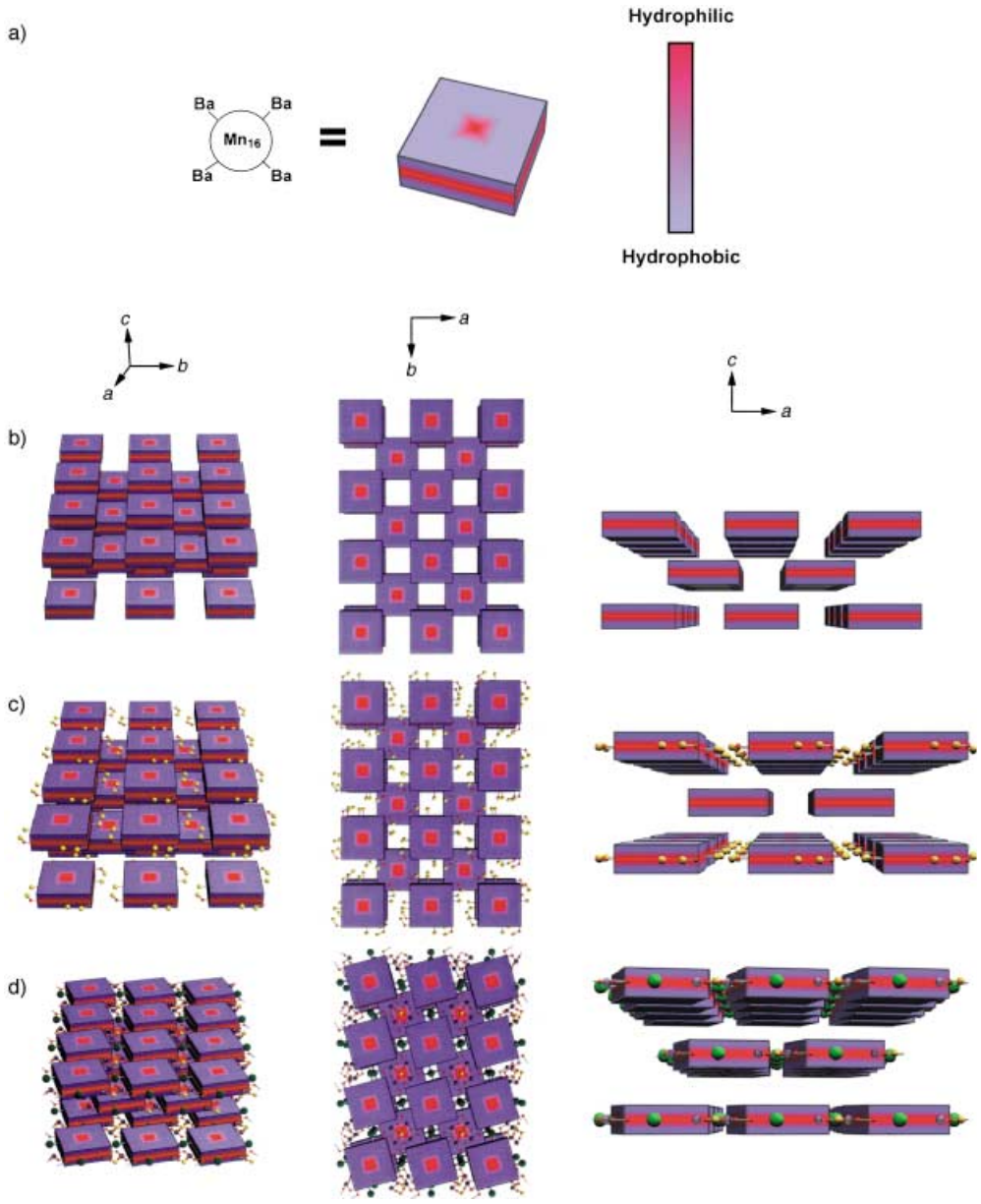

Figure 4. Comparative packing diagrams of P1, P2, and P3 phases. Peripheral Ba^{2+} and Na^{+} ions are shown as spheres, colored as in Figure 1. a) Representation of P1 as a block with 4/*m* symmetry, and hydrophobic (ligand L backbone) and hydrophilic (H_2O and carbonyl oxygen atoms) regions. b) The P1 phase. c) The P2 phase. P1 layers alternate with Unit 2 layers that contain additional Na^{+} ions. d) The P3 phase, including the peripheral Ba^{2+} and Na^{+} ions.

only one compositional degree of freedom (NaCl concentration) is varied, phase P2 is specific to H_2O.

The relationship between the isotope type and NaCl concentration is not entirely clear. However, as shown in Figure 2, the heavy isotopologue appears to compensate to a certain extent for a diminished NaCl concentration. The formation of phase P3 at higher NaCl concentrations in H_2O, and of phase P1 at lower NaCl concentrations in D_2O, is consistent with this notion. This effect could be due to differences in solvation numbers and osmotic and activity coefficients observed for NaCl solutions in D_2O and H_2O.[9] The composition (NaCl concentration)–isotopologue equivalency, however, cannot explain the formation of P2 only in H_2O, or the differences in crystallization times. Other factors, such as hydrogen bonding and the more organized "structure" of liquid D_2O[10] may also play a role.

Differences in hydrogen bonding is an interesting possibility considering that formation of a solid-state phase in only one type of water is known for ice, namely the high-pressure ice IV phase being identified only for D_2O.[5] Hydrogen bonding, if important in this case, is expected to manifest itself ultimately in the structure of the ordered water molecules within the Mn_{16} crystalline lattices. However, the degree of association (or even existence) of the Mn_{16} phases in solution is not known, while a variable degree of disordered water molecules are present in the solid-state within the same, well-

defined molecular architectures. Alternatively, hydrophobic effects, attributed to the organic ligand backbone, may play a role. Thus, it is known that the self-association of both α-chymotrypsin[11] and some antibodies[12] is enhanced as the solution ionic strength is increased by the addition of NaCl. This enhancement, which is not due to specific ion interactions, is entropically driven, and was ascribed to hydrophobic effects.[12] Similar to the case of the Mn_{16} aggregates, a change from H_2O to D_2O has the same effect as an increase in NaCl concentration, namely a higher degree of self-association, an observation consistent with the notion that hydrophobic effects are stronger in D_2O.[13] Whether the hydrophobic effect is the common denominator for the above biological effect and the parallel relationship between deuterium content and ionic strength we observe for inorganic associations, remains to be determined. If the answer is affirmative, then the hydrophobic effect may have synthetic value in the rational design of mixed organic–inorganic aggregates.

In summary, isotope-induced structural effects manifest themselves primarily in the assembly of two supramolecular architectures through the incorporation, or lack of incorporation, of additional ions, an effect that is mimicked by increases, or decreases in ionic concentrations, respectively. A third, structurally intermediate solid-state material forms in H_2O, but not in D_2O. The topologies and nuclearities of polynuclear metal oxo/hydroxo aggregates, that can seldom be predicted, let alone controlled, might be tuned, perhaps even in a rational way, with the help of isotope effects. Unique, isotopologue-specific aggregates may also be obtained.

Experimental Section

The synthesis of Mn_{16} clusters was performed as previously reported,[3] in both H_2O and D_2O, except that amounts of NaCl, ranging from 0.300 g to 5.00 g, were dissolved in each solution. Crystalline materials were dried briefly and subjected to multiple, standard iodometric titrations for the determination of average Mn oxidation states. The results are reported with standard errors that incorporate a possible 10% uncertainty in the amount of water of hydration. Single-crystal X-ray studies were performed at low temperature by using standard procedures. The number of disordered water molecules was estimated from the total electron density present in the structural voids. Magnetic susceptibility measurements of microcrystalline samples were performed in a constant field of 10000 G using a Quantum Design SQUID MPMS 5L magnetometer. The samples were briefly dried in air, sealed in plastic containers and inserted into the SQUID magnetometer, which was prestabilized at 5 K. Several data sets, which were collected between 5 and 300 K in both temperature ascending and descending modes, gave identical results. No difference was observed even after storing the sealed samples for 4 h at room temperature. Diamagnetic corrections were calculated using Pascal's constants.

For the complete crystallographic data for P2, see the Supporting Information. CCDC-199051 (P1), CCDC-192461 (P2), and CCDC-199050 (P3) contain the supplementary crystallographic data for this paper. These data can be obtained free of charge via www.ccdc.cam.ac.uk/conts/retrieving.html (or from the Cambridge Crystallographic Data Centre, 12, Union Road, Cambridge CB21EZ, UK; fax: (+44) 1223-336-033; or deposit@ccdc.cam.ac.uk).

Received: September 19, 2002
Revised: January 27, 2003 [Z50200]

Keywords: aggregation · isotope effects · manganese · supramolecular chemistry

[1] J. A. K. Harmony, R. H. Himes, R. L. Schowen, *Biochemistry* **1975**, *14*, 5379.
[2] R. Radfar, A. Leaphart, J. M. Brewer, W. Minor, J. D. Odom, R. B. Dunlap, C. R. Lovell, L. Lebioda, *Biochemistry* **2000**, *39*, 14481.
[3] J. Lee, N. D. Chasteen, G. Zhao, G. C. Papaefthymiou, S. M. Gorun, *J. Am. Chem. Soc.* **2002**, *124*, 3042.
[4] The Mn oxidation states are better determined by X-ray absorption spectroscopy. See: M. M. Grush, J. Chan, T. L. Stemmler, S. J. George, C. Y. Ralston, R. T. Stibrany, A. Gelasco, G. Christou, S. M. Gorun, J. E. Penner-Hahn, S. P. Cramer, *J. Am. Chem. Soc.* **1996**, *118*, 65. Such measurements are planned in collaboration with Dr. Serena DeBeer George.
[5] "The Hydrogen Bond in Ice": E. Whalley in *The Hydrogen Bond* (Eds.: P. Schuster, G. Zundel, C. Sandorfy) North-Holland, Amsterdam, **1976**.
[6] a) X-ray data for P3 from H_2O. The unit cell parameters of P3 from H_2O are similar.[3] Tetragonal, $I4/m$. Unit cell dimensions at $T=173(2)$ K: $a=20.9287(10)$, $c=26.788(3)$ Å; $V=11733.4(15)$ Å^3; $Z=2$. Data/restraints/parameters: 6854/0/344. R indices, $[I>2\sigma(I)]$: $R1=0.0450$, $wR2=0.0981$; b) X-ray data for P1 from D_2O. The unit cell parameters of P1 from H_2O are similar.[3] Tetragonal, $I4/m$. Unit cell dimensions at $T=173(2)$ K: $a=25.296(4)$, $c=20.565(4)$ Å; $V=13159(4)$ Å^3; $Z=2$. Data/restraints/parameters: 6008/0/293. R indices, $[I>2\sigma(I)]$: $R1=0.0725$, $wR2=0.1629$.
[7] X-ray data for P2. Tetragonal, $P4/m$. Unit cell dimensions at $T=173(2)$ K: $a=23.583(2)$, $c=22.539(3)$ Å; $V=12535(2)$ Å^3; $Z=8$. Data/restraints/parameters: 11356/0/788. R indices, $[I>2\sigma(I)]$: $R1=0.0532$, $wR2=0.1449$.
[8] a) R. T. Stibrany, S. M. Gorun, *Angew. Chem.* **1990**, *102*, 1195; *Angew. Chem. Int. Ed. Engl.* **1990**, *29*, 1156; b) S. M. Gorun, R. T. Stibrany, A. Lillo, *Inorg. Chem.* **1998**, *37*, 836.
[9] a) O. D. Bonner, G. B. Woolsey, *J. Phys. Chem.* **1968**, *72*, 899; b) O. D. Bonner, *J. Am. Chem. Soc.* **1970**, *92*, 4197.
[10] P. Mukerjee, P. Kapauan, H. G. Meyer, *J. Phys. Chem.* **1966**, *70*, 783.
[11] K. C. Aune, L. C. Goldsmith, S. N. Timasheff, *Biochemistry* **1971**, *10*, 1617.
[12] J. M. R. Moore, T. W. Patapoff, M. E. M. Cromwell, *Biochemistry* **1999**, *38*, 13960.
[13] G. C. Kresheck, H. Schneider, H. A. Scheraga, *J. Phys. Chem.* **1965**, *69*, 3132.

